Printing Semiconductors by Orthogonal Separation of Reactive Precursors

A Major Qualifying Project Report
In partial fulfillment of the requirements for the
Degree of Bachelor of Science in Chemistry and Mechanical Engineering
Submitted to the Faculty of

Worcester Polytechnic Institute
100 Institute Road
Worcester, Massachusetts 01609

Submitted By:
Angel D. Fernandez Sorondo

Date:
April 28, 2022

Table of Contents

List of Figures

List of Tables

Glossary

FTO Fluorine-Doped Tin Oxide
TEA Triethanolamine

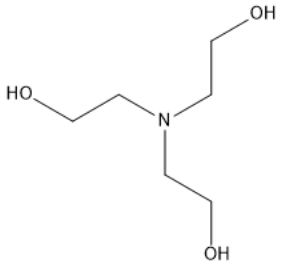

STA Silico-tungstic Acid

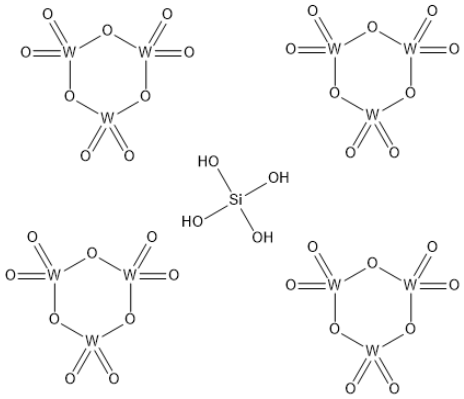

XPS X-Ray Photoelectron Spectroscopy
XRD X-Ray Diffraction

Abstract

This project focuses on the development of precursors for inkjet printing of semiconductors, specifically stibnite (Sb_2S_3). For inkjet printable semiconductors one issue is the maintenance of extrusion area of the printer, where the nozzle could continuously get clogged due to growth and clumping. To combat this, the developed precursors would be extruded and deposit the semiconductor onto a glass surface. Structural and electronic properties of stibnite were analyzed using x-ray photoelectron spectroscopy and x-ray diffraction. Surface tension and viscosity measurements were done to match the thermofluidic requirements the precursors would need to for an existing inkjet printer.

Background

The field of printable semiconductors has only recently been researched and finally put into application. The field of printable electronics is a promising approach for the future in electronics due to the versatility of applications, such as thin film transistors, displays and 3D electronic structures. Future studies have explored the digital writing capabilities of functional materials, but current capabilities lack in optimization of to achieve fine feature sizes with high performance. Common challenges that current commercially available inkjet printer heads are larger than some applications require, that the droplet sizes can cause extrusion to not be as constant as to create a line but rather they may spread to a larger localized area, and deterioration in optical and electronic properties of the semiconductor.[6][10][11]

Through various studies on the development of semiconductors, metal sulfides have shown to be promising compounds in semiconductor deposition for its use in solar cell application, for containing inexpensive reagents for semiconductor formation, and reduced impedance on printer maintenance, as they can be separated to control deposition. Thorough this project. stibnite, or more commonly referred antimony sulfide, was optimized to fit conditions of an existing inkjet printer.

Experimental Section

2.1 Chemicals

All water was provided by a Millipore Milli-Q system at 18 MΩ cm resistivity. Antimony potassium tartrate hydrate (98%, Alfa Aesar), thioacetamide (99+%, ACROS Organics), ammonium hydroxide (28% aqueous, Alfa Aesar), silico-tungstic acid (≥99%, Sigma Aldrich), ethylene glycol (Oakwood Chemical). Triethanolamine (97%, ACROS Organics) was prepared into a 50% v/v and an 80% v/v aqueous stock solution.

Other stock solutions were created when progressing to a two solvent system. For those experiments two groups of stock solutions were prepared: one group of stock solutions vary the concentrations of antimony potassium tartrate hydride and silico-tungstic acid using ethylene glycol as a solvent, and the other group varying thioacetamide, ammonium hydroxide, and triethanolamine concentrations.

2.2 Bath Deposition of Stibnite

Stibnite (Sb_2S_3) depositions initially were based on established procedures.[14][17] The initial procedure was done in an aqueous system having using 1 g antimony potassium tartrate hydrate, 15 mL 0.1M thioacetamide, 3 mL 10μM silicotungstic acid, 1.8 mL 28% ammonium hydroxide, and 6 mL 50% triethanolamine aqueous stock solution, within 48 mL of water. The mixture was then pipetted into plastic centrifuge tubes containing a substrate for deposition. The centrifuge tube was closed and left out in air at room temperature for about 40-48 hours. During this deposition cycle the solution would begin from murky light yellow and transition into a darker orange and then a deep maroon color. In many written procedures the bath was typically heated but the deposition process will be applied to an inkjet printer for semiconductors which would be in room temperature environment.

After a deposition cycle, the solution was poured off and the substrates were placed into an annealing furnace with nitrogen purge flow, ensuring to not let anything contaminate the glass deposited surface. On the centrifuge tube there were some films grown on the sides where in contact with the solution. After purging atmosphere from the furnace, it was heated to 300°C over the course of an hour. After cooling down the substrates were then stored on aluminum foil in a Petrie dish.

Substrates were then deposited and annealed for a second time utilizing the same procedures mentioned. Initial trials with only one deposition and annealing procedure, showed to have poor adhesion and poor photovoltaic properties.

Other experiments have been done to improve adhesion properties. These experiments are varied thioacetamide, ammonium hydroxide, and triethanolamine concentrations. The variation of heat was also studied but mostly disregarded due to the nature of the target system. The best set of conditions that created more adhesive films was made with 500 mg 98% antimony potassium tartrate hydrate, 60 mg thioacetamide, 40 mg silico-tungstic acid, 1 mL of 28% aqueous

ammonium hydroxide, and 1.5 mL of 80% triethanolamine v/v with water, along with an additional 17.5 mL of water.

2.3 Separation of Reactive Precursors

The goal of this project is to develop a method to deposit semiconductors onto a surface rather having a semiconductor be extruded from the nozzle of an inkjet printer. Through the studies conducted through the bath deposition process, two precursors are to be created containing various mixtures of the reagents and solvents to compare films grown on the FTO glass slides. Changes in reagents include variations on triethanolamine concentrations with water and ethanol, use of ethanolamine rather than triethanolamine, changes in solvent using ethylene glycol, ethanol, water, or mixtures of such.

Along with variation in initial reagents and their quantities, studies on the deposition temperature, annealing procedures, and surface variations were studied. In terms of deposition temperature literature states that the best deposition process would occur under 80ºC but with the unknown conditions of the printer, temperature studies were conducted between room temperature and 50ºC. Annealing temperatures and procedures were also varied. Through some literature procedures they suggest that the annealing time should be done at 300ºC for 5 minutes and others suggested that the annealing process should be consistently at 300ºC for an hour. Through the large variation in time studies varied the ramping up time, time of constant temperature, and cool down rate.

Finally, the last characteristic that was varied in this process is conformation of the reactive surface. One procedure tested is defacing the surface to ensure a rough surface for a crystal to grow; this was done by scratching the surface with sandpaper or with a metal spatula. Another method for reconfiguring the surface is done by the application of a precursor on the surface for the adhesion of one of the semiconductor components. Through this process an initial precursor was spin deposited at 2500 rpm, for a variable number of times, allowing the surface to initiate contact with a precursor creating a layer for the next precursor to deposit on. Afterwards the second precursor will be applied, then later that initial precursor will be applied to allow proper formation of the complex.

2.4 X-ray Photoelectron Spectroscopy (XPS) Methods

A PHI5600 XPS system acquired x-ray photoelectron spectra data scanning stibnite deposited thin films.[3][5] In few experiments the substrates required charge potentially for poor adhesion to carbon tape applied on the film for continuous conductivity. Wide-energy range surveys on samples determined elements present on the substrate that were supplement ed by high-resolution scans of the C 1s, O 1s, N 1s, S 2p, Sb 3d, Sb 4d, K 2p, W 4f, Si 2p regions. All features were fit to a GL(30) peak shapes with a W Toguard background. Features in the C 1s, K 2p, N 1s, S 2p, Si 2p regions were constrained to a full-width-at-half-maximum values (fwhm) values for each element. Features in the Sb 3d and Sb 4d contain fall under the same binding energy as the O 1s and the W 4f regions respectively, thus those regions will have separate fwhm

values. Peak separations values for S 2p and Sb 3d regions are 1.18 eV and 9.34 eV respectively per literature values.

2.5 X-ray Diffraction (XRD) Methods

Another method of the surface characterization is through x-ray diffraction. X-ray diffraction is a nondestructive technique in which an x-ray beam is transmitted onto a surface and then collected on an area detector. The diffraction pattern is made from reflections from the varying orientations of a sample. The varying intensities of the reflections can be used to determine structures of crystals. A D8 Focus Bruker-axs pXRD (powder x-ray diffractometer) was used to characterize the stibnite films produced in which the voltage and current were set to 40 V and 10 mA. Since the films were deposited on a thick piece of fluorine-doped tin oxide (FTO) slide the stage and set had to be adjusted to place the sample in the line of the x-ray beam. An image of the how the slide is shown below in Figure 1.

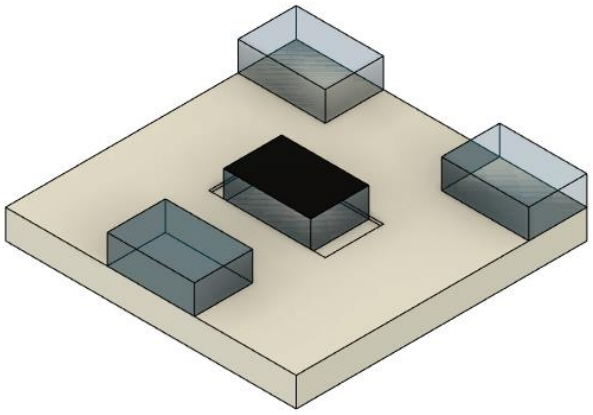

Figure 1:This image depicts the puck that would be set for the stage of the pXRD. The stage has three points of contact on the corners held where the glass slides are on the plane. In the center slot is the loading area for the sample.

2.6 Rheometer Methods

When implementing inks into the inkjet printer, one must ensure that the inks fit certain criteria for proper extrusion of the inks. The inks are to be accommodated to a Dimatix Fujifilm DMP-2800 Series Printer which requires that the inks extruded should have a viscosity within a 2-30 cP range. To ensure that the inks fit under those conditions, a rheometer was used to generate plots comparing the viscosity to the shear rate of the precursors.

The rheometer used for this analysis is a Discovery HR-2 Hybrid Rheometer. Viscosities were also measured in relation to temperature. Temperature has an inverse relationship with viscosity in which as temperature increases a fluid becomes less viscous. Setting the rheometer disk to have free spinning, the viscosity data was collected with temperature intervals of 20 ºC, beginning at 30 ºC and ending at 70 ºC under shear rates from 0 to 3000 Hz as to ensure that the precursors would have similar viscosities under certain extrusion rates.

2.7 Tensiometer Methods

Once an ink is extruded from the inkjet printer, the ink will need to maintain a conformation to localize the deposition process. In doing so studying of the surface tension of each ink has been done with a [insert tensiometer model]. [insert tensiometer model] has the capacity to vary the temperature of its chamber for creating relationships between the surface tension and temperature. For this experiment a droplet was hung from the tip of a syringe and through comparing the area and predicted volume of the droplet surface tension was measured at 30-70°C in intervals of 10°C. Surface tension measurements were done at these conditions due to the inkjet printer having a maximum chamber temperature of 60°C and understanding the relation that the temperature change in the environment has on maintaining a controlled.

2.8 Final Procedure

Stibnite depositions for the application of inkjet printing was done through the creation of two reactive precursors, one containing antimony and the other introducing sulfur into the system. The antimony precursor was made by using 610 mg of 98% antimony potassium tartrate hydride and 70 mg of silico-tungstic acid within 40 mL of ethylene glycol. This solution needs to be agitated until the solids completely dissolve. The sulfur-containing solution is made using 160 mg of thioacetamide, 3 mL of a 4:1 ratio of triethanolamine and water, 3 mL of 28% aqueous ammonium hydroxide, in 14 mL of ethylene glycol and let sit until solution goes from a clear solution to a green solution.

The preparation of a fluorine doped tin oxide (FTO) glass slide will be prepared through spin deposition process. Droplets of the antimony containing precursor will be placed on the surface of the slide and the slide will be spun at a rate of 2500 rpm. This process will be repeated ten times as to ensure a antimony layer is adhered on the surface on the glass.

Afterwards a droplet of the sulfur containing solution was placed on the surface with a 10 μL pipet and let to rest for an hour until the same process was done with an additional droplet of the antimony containing solution. This process was done by heating environment to 50°C and let to rest for 24 hours. During this deposition time the formation of an orange precipitate will appear and over time will disappear throughout the deposition process. Unlike with the bath deposition where the complexes formed in solution will continue to change and undergo a color shift from yellow to orange to a dried blood color, this droplet deposition will create an orange complex and over time it will disappear.

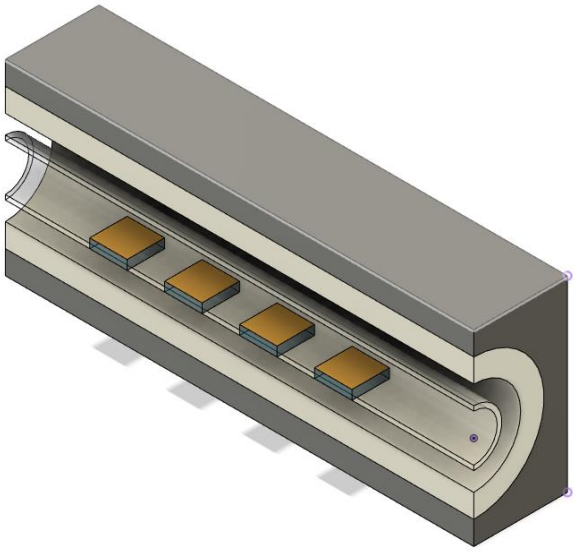

Figure 2: Tube furnace configuration. Inner cylinder is a borosilicate glass tube surrounded by insulation. The slides were place in the glass tube with an inert gas flowing through the tube.

After the 24-hour deposition time the slides were placed in a tube furnace, depicted above in Figure 2, annealed under and inert gas flow. Nitrogen or argon gas was sent through the tube prior to the insertion of the slides as to expunge any excess oxygen in the tube. The slides were then annealed ramping the heat to 300ºC for 8 minutes and maintaining that temperature for 15 minutes. Afterwards there was a slow ramp back down to room temperature for 37 minutes. Once complete the slide should have a black/dark brown film on it.

Results and Discussion

3.1 Stibnite Deposition in an Aqueous Bath

3.1.1 Initial Aqueous Deposition Results

Beginning the experimentation process, studies for aqueous deposition began with repetition of an existing procedure. Following the procedures set out in Section 2.1, two deposition cycles were done under the conditions laid out. Through x-ray photoelectron spectroscopy and x-ray diffraction initial characterizations of this initial procedure are outlined in Figure 3 and Figure 4 respectively. Along with these traces a predicted calculated trace is presented in Appendix B.

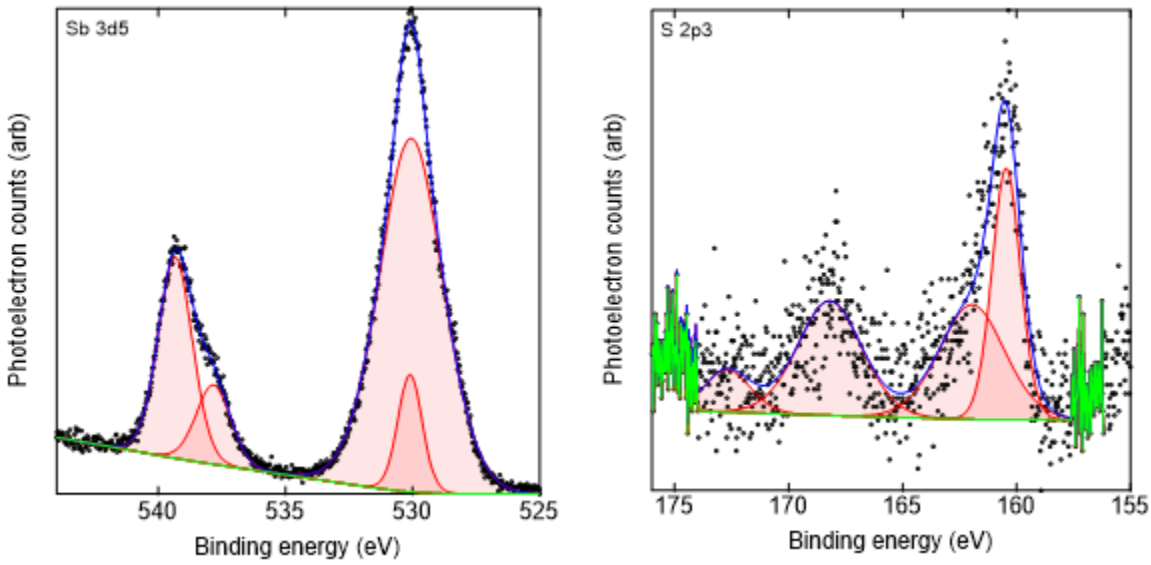

Figure 3: This is the x-ray photoelectron spectra of an initial aqueous deposition for stibnite, where antimony (left) and sulfur (right) are shown here. Within these spectra it is shown that a sulfide compound is created on the film due to the positioning of the 3d5/2 (right) peak on the antimony spectra and a set of peaks starting at 160 eV in the sulfur spectra. Alas, oxygen and other contaminates are on the surface demonstrated by the left set of peaks in the sulfur spectra and a deformity of the 3d3/2 peak in the antimony graph, with an unacknowledgeable peak hidden within the 3d5/2 peak.

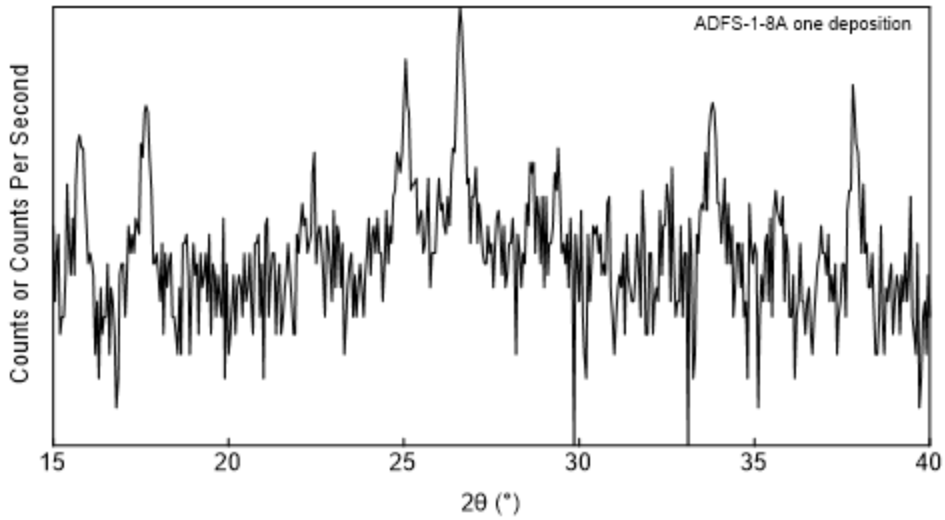

Figure 4: X-ray diffraction trace of stibnite after once cycle within aqueous deposition. Peaks indicate the presence of stibnite as well as potential oxide contaminates.

Following these initial procedures, variations on that initial procedure beginning with changes in initial reagent quantities. For comparison for these experiments the rates of reaction were measured, and quantity of the reagents were measured. As mentioned in in Section 2.1 when undergoing the bath deposition, the complexes formed are visibly present while undergoing a color shift from yellow to orange and finally to a dried blood color. The color of the complex that creates the most ease in the formation of the deposition process is the orange complex, the dried blood complex may represent an oxidized version of the complex. Initially concentrations of the thioacetamide and antimony potassium tartrate hydride were varied to compare thickness of the film after a cycle. After comparing the variation of the reagents introducing the main components of stibnite, it was found that film thickness did not increase, but with increasing concentrations of thioacetamide a greater area of film adhered to the surface than the initial procedure but with the addiction of the extra thioacetamide precipitate formed in solution. Below in Figure 5 depicts traces of stibnite films which have gone deposition under varying thioacetamide concentrations, which show that variation of the of stibnite did not create an effect on characterization.

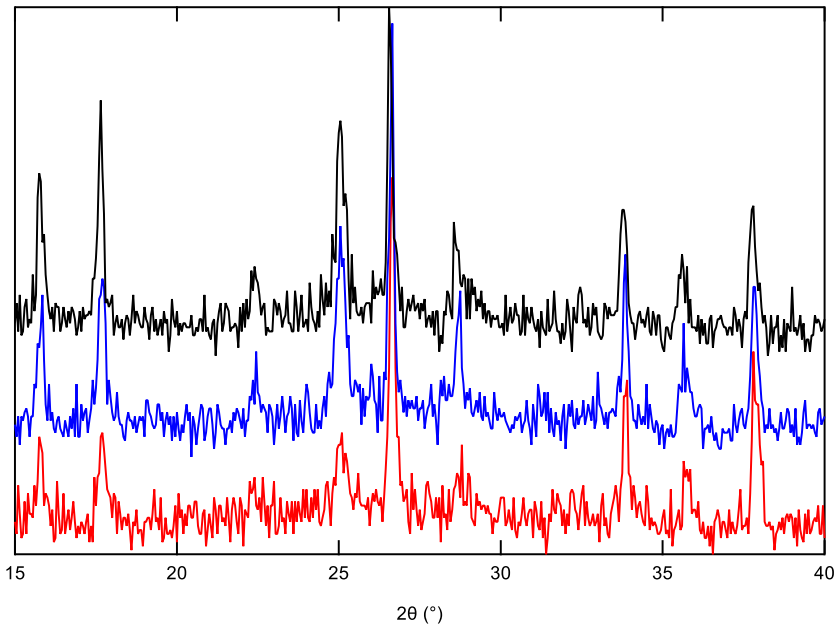

Figure 5: Within this figure there are three traces for the comparison of stibnite. In optimization of stibnite deposition variations of thioacetamide have shown to create films on a larger area consistently. In the traces depicted above films have been created under 1x (red), 1.5x (blue), and 2x (black) which show that in each case stibnite can be characterized, where the blue and black traces form larger counts than the red trace.

3.1.2 Optimization of Aqueous Deposition

Comparisons of the previous two experiments were done using Design of Experiments with the initial goal of formation of a film on the surface, and proper characterization of stibnite on said films. While varying all components described previously there were many instances that lead to a lack of film adhering to the surface or with poor characterization. As seen in the previous section many films could adhere to the surface and may produce impurities onto the surface. As a result, the recipe that led to a more consistent film for a bath deposition is made with 250 mg of 98% antimony potassium tartrate hydrate, 80 mg of thioacetamide, 40 mg of silico-tungstic acid, 1.5 mL of a 4:1 ratio of thioacetamide to water, and 1.5 mL of 28% ammonia hydroxide.

3.2 Solvent Variation for Droplet Deposition

Beginning the reconfiguration process, printer specifications were not initially known. Through this process precursors were made varying solvents and solvent mixtures to create various functional possibilities for printer applications. Although initial procedures indicate the use of water as a solvent, water cannot be used as a solvent for printing applications due to its low viscosity. Solvents and solvent mixtures with greater viscosities were used such as ethylene glycol, and mixtures of ethylene glycol, water, and ethanol. As previously stated in the experimental sections, drops of precursors were placed onto the slide to localize deposition; shown in Figure 6 and Figure 7 there XPS spectra of two promising examples, pure ethylene glycol as a solvent and a 50/50 by volume mixture of ethylene glycol and ethanol respectively.

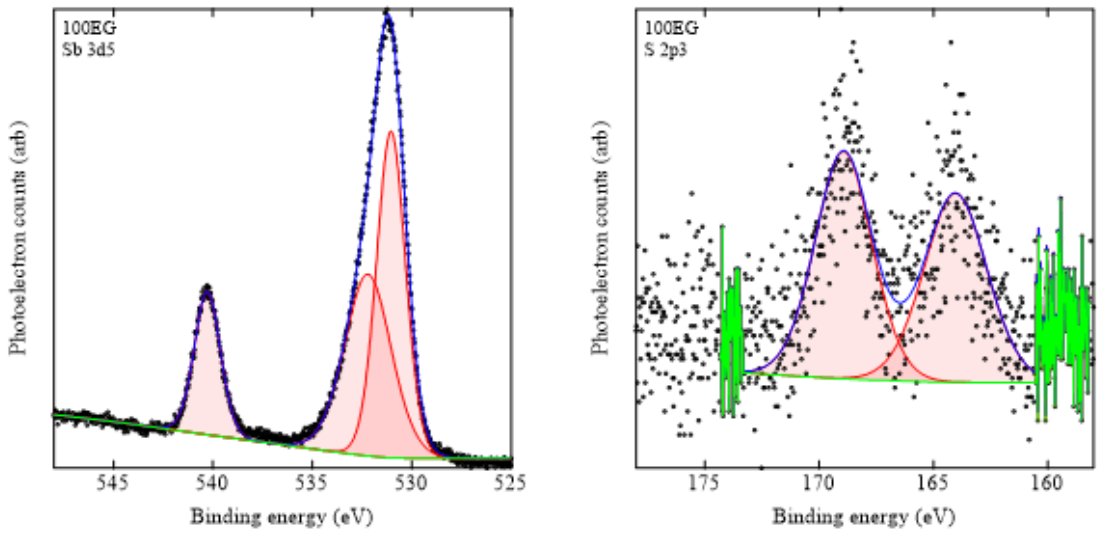

Figure 6: Representing x-ray photoelectron spectra for antimony (left) and sulfur (right) for a droplet deposition of stibnite in ethylene glycol as a solvent. In the antimony spectra, within the 3d5/2 peak (large right peak) a peak for oxygen appears as a contaminate in the sample which can be attributed to the formation of antimony oxides. On the right spectra, sulfur is shown to be present as a sulfide but as with antimony sulfur forms a compound with oxygen creating sulfate compounds.

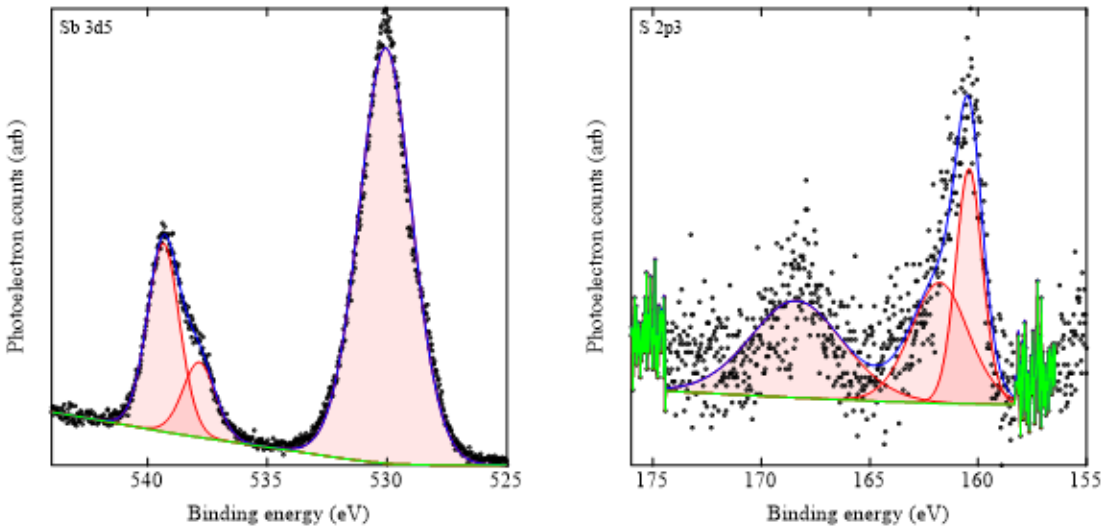

Figure 7: X-ray photoelectron spectra for identifying antimony (left) and sulfur (right). This spectrum is for a droplet deposition with a equal volume solvent mixture comprised of ethylene glycol and ethanol. In the left spectra we see that antimony is abundantly present within the sample with some slight contamination on the 3d3/2 peak. On the right spectra sulfur is shown to be present, but within the shifted peaks there are sulfate, sulfite, and sulfide compounds present.

These two figures demonstrate that antimony and sulfur can form to create a metal sulfide complex, but due to being in atmospheric conditions, and with water partially in solution, oxygen contaminants would fit within solution creating metal oxide and sulfate/sulfite compounds.

3.3 Surface Characteristics of FTO Slides

3.3.1 Physical Deformation of the FTO Slide Surface

During some depositions there were many cases where the deposition process did not adhere to the surface of the FTO slide. Following some crystallization processes, like with pure water, a physical deformity, or a rut, was created with sandpaper or a simple scratch onto the surface of the FTO slide to potentially allow an ease in initiating crystalline growth. Unfortunately, through this process with any droplet deposition procedure, no depositions adhered to the surface of the film and after the annealing process the slides were blank canvases.

3.3.2 Spin Deposition of One Precursor

Another process for surface preparation for the growth of stibnite crystals is preparing the surface with one component of the crystal. Through this process individual precursors were dropped onto one of the FTO glass slides, and the slide with the droplet was spun. As stated in Section 2.3, the precursors were initially dropped onto the surface and then spun. This procedure was repeated 5 times through this experiment and while analyzing the surface of the slide prior to the addition of precursors used for deposition. Shown in the two figures below, Figure 8 and Figure 9, are XPS spectra of the surfaces after the application of an antimony and sulfur precursor respectively. Looking at the spectra produced what is shown initially in both spectra there is a great oxygen contamination in the creation of metal oxide and sulfate complexes, due to the surface of the substrate being oxygen. Within the antimony-initiated substrate, Figure 8, there is a clear presence of antimony on the surface due to the $3d_{3/2}$ peak clearly present. The $3d_{5/2}$ peak for antimony is covered by the amount of oxygen present directly beneath the antimony layer. Within the sulfur-initiated substrate, Figure 9, the peaks blend in within the noise within the background. From the predicted peaks, shown is the formation of sulfide and sulfate compounds on the surface. From this one can see that with an antimony-containing precursor should be used when initiating the spin deposition.

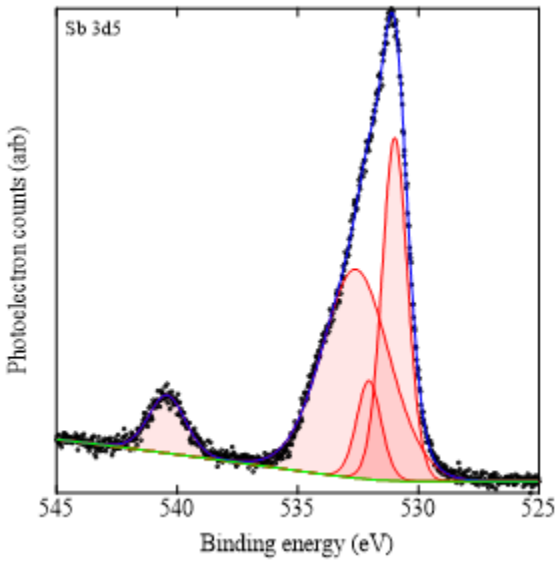

Figure 8: XP spectra of antimony of an FTO slide which has been spin deposited with an antimony containing precursor. With such a sparce film applied, oxygen overpowers the intensity of the binding energy near 531 eV. This spectra indicates that antimony may have crated an oxide compound onto the surface.

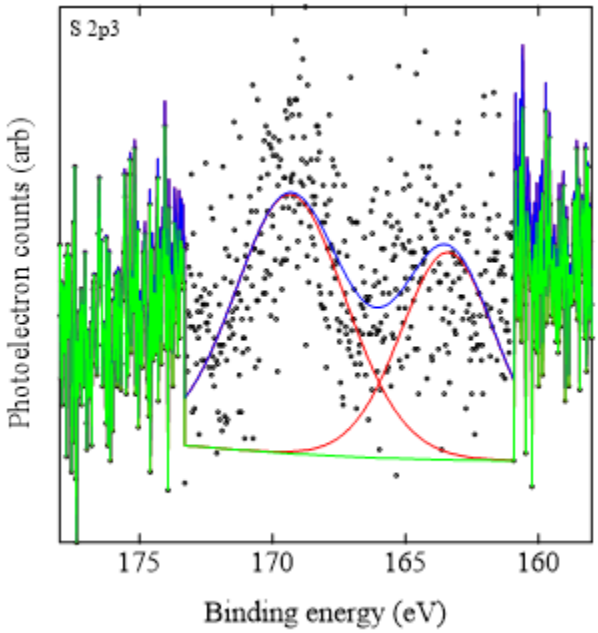

Figure 9: XP spectra of sulfur after an FTO glass slide has been spin deposited with a sulfur containing precursor. This figure may demonstrate the existence of sulfate and sulfide compounds formed on the surface. The size of the sulfur peaks hide within the noise surrounding it, not creating a secure foundation to distinguish the potential sulfur peaks from the noise.

From these conditions presented above, the final procedure begins with the spin deposition of the antimony-containing precursor, leading into the application the combination of both precursors. After completing the annealing process, the films produced generate the XP spectra shown below in Figure 10. Within these spectra antimony and sulfur undergo a shift up-field by 2 eV,

potentially due to poor conductivity, but demonstrate that oxygen is not as present within the sample. In the antimony spectra the $3d_{5/2}$ peak, after the shift, falls under the area indicating an antimony sulfide compound formation, as with the sulfur spectra.

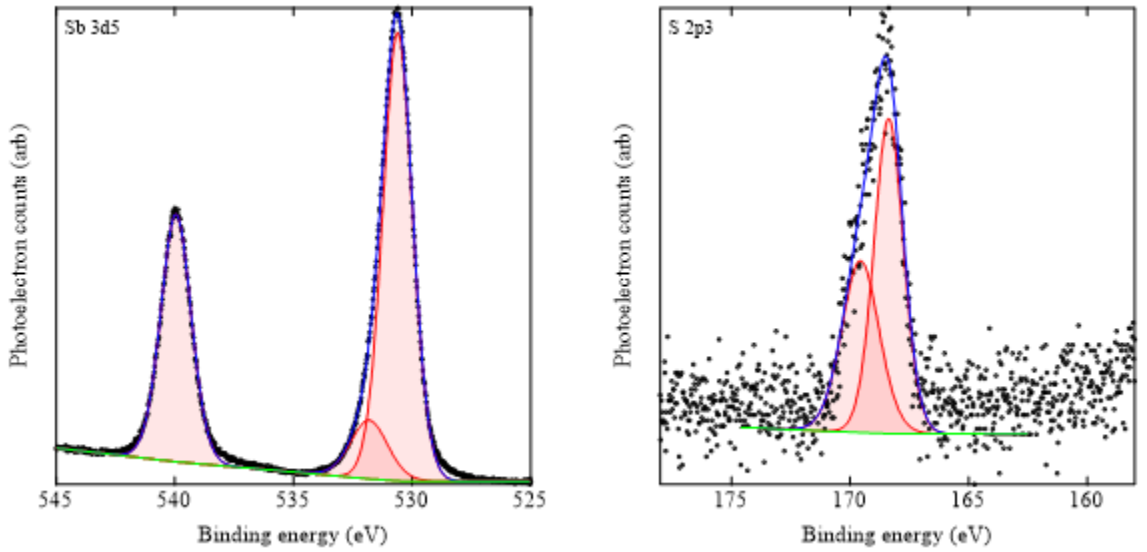

Figure 10: These are x-ray photoelectron spectra for the final procedure for stibnite deposition. The left spectra is within the antimony range and the right spectra is within the sulfur range. These spectra are shifted up by approximately two eV due to poor adhesion to improper conductivity between the sample and the puck. Within the antimony spectra oxygen seems to be slightly present in comparison to antimony, potentially covering any antimony oxide compounds registered. Within the sulfur spectra on the right, the sulfur creates a cleaner peak than in previous instances. Along with the shift the peak can be characterized to create a sulfide compound.

3.4 Conforming Precursors to Inkjet Printer Specifications

3.4.1 Rheometer Measurements

The precursors created are made with ethylene glycol as the main component for the solvent, making 100% and 70% of the antimony-containing and sulfur-containing precursors respectively. Literature states that ethylene glycol should have a viscosity of approximately 16 cP at room temperature, and Ammonia and triethanolamine should have viscosity values of 1.7 cP and 590 cP at room temperature respectfully. The sulfur-based solution comprised of a 14:3:3 mL mixture of ethylene glycol: 28% aq. Ammonium Hydroxide: 80% Triethanolamine is expected to have viscosity values resembling ethylene glycol as the main component in the solution.

As mentioned in Section 2.6, viscosity measurements were collected while varying the shear rate and temperature. Below in Figure 11 depicts the viscosities both the antimony containing and the sulfur containing solutions. The expected trend for viscosity in relation to temperature is when temperature increases the viscosity decreases which is shown for both solutions. With the antimony containing precursor the viscosity is around the expected viscosity for ethylene glycol maintaining a viscosity at around 15 cP throughout the various shear rates. The sulfur-containing

precursor is shown to be less viscous with a viscosity approaching 4 cP as the shear rate increases. For inkjet printing purposes the inkjet printer requires inks to have a viscosity within 2-30 cP in which both solutions fit within the range.

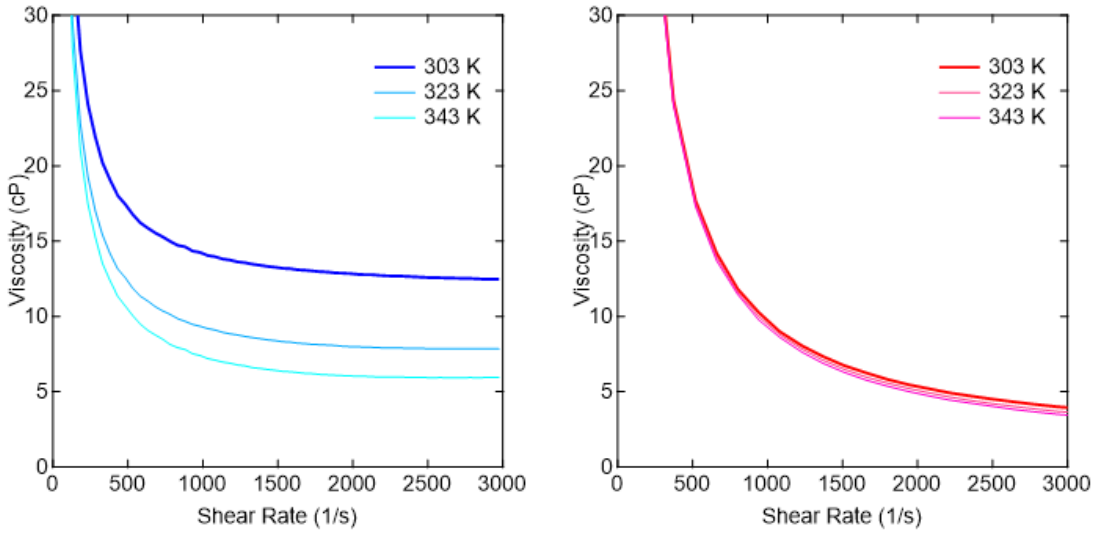

Figure 11: Depicted above are plots of the viscosity of the antimony containing precursor (left) and the sulfur containing precursor (right) compared to the shear rate of the rotating disk.

3.4.2 Tensiometer Measurements

Measurements of the surface tension were conducted on the developed precursors. Literature values for the surface tension for the main components of each precursor, i.e. ethylene glycol, triethanolamine, and water, are 48.4 mN/m, 48.4 mN/m, and 72.7 mN/m at room temperature respectfully.[1][9][23] For this study the relationship between the surface tension and the temperature were done. Below in Figure 12 and in Table 1 and Table 2 shows that relationship for the antimony and sulfur containing precursors.

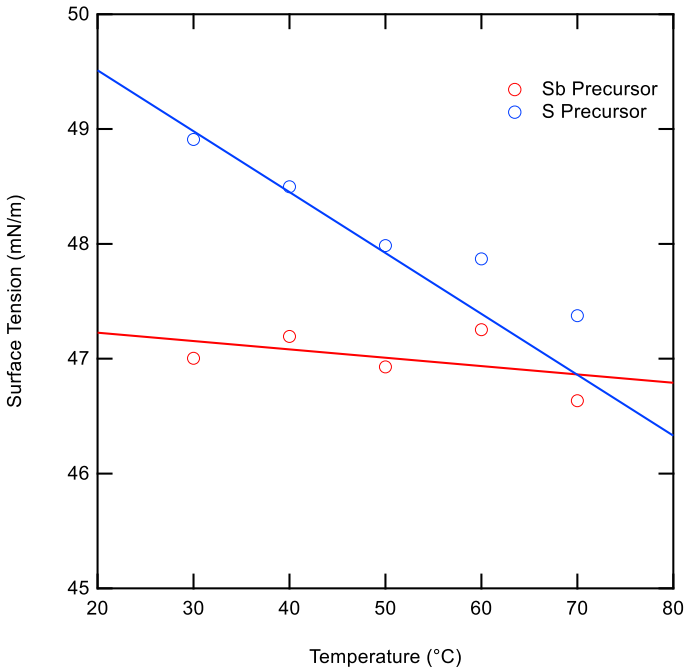

Figure 12: Relationship between surface tension of the precursors in relation to temperature. The average surface tension values for the antimony precursors are marked in red and the sulfur containing precursor are marked in blue. Each set of points have a trendline associated with the data.

Temperature (ºC)	Surface Tension (mN/m)
30	47.004
40	47.19467
50	46.928
60	47.253
70	46.6345

Table 1: Surface tension values in relation to temperature for the antimony containing precursor

Temperature (ºC)	Surface Tension (mN/m)
30	48.910
40	48.498
50	47.985
60	47.870
70	47.374

Table 2: Surface tension in relation to temperature for the sulf4ur containing precursor

Literature says that the surface tension should decrease as the temperature increases, due to increased energy within the droplet. For the antimony containing precursor that relation falls to be true but not to a large extent as the surface tension at each temperature seems to hover around 47 mN/m. The sulfur containing precursor, although being a mixture of ethylene glycol, triethanolamine, water, and ammonia the surface tension for this mixture is larger than that for pure ethylene glycol, and clearly fallows the negative correlation at a higher rate.

Conclusions and Future Work

A variety of precursors were prepared for controlled deposition of stibnite (Sb2S3) on fluorine-doped tin oxide glass surfaces. The deposited films were characterized by photoelectrochemistry and x-ray diffraction and the precursors were fit measured and fit to the thermofluidic properties of an inkjet printer through rheometer and tensiometer analysis. While this work demonstrates their versatility of the deposition process, the work done has produced several cases of incorrect films produced or have not produced films under various conditions. In many cases, precursors were mad that could deposit a stibnite film, such as the precursors created with ethanol various concentrations of ethanol, but alas they did not conform to the inkjet printer specifications.

Future studies should include mechanism study on the deposition process. As found pH influences the quality and rate of complexes formed in deposition. To control this rate and better understand the deposition mechanisms and better understanding of the adhesion properties of the surface. For improved surface adhesion suggestions are using silanes, such as mercaptoprosyltriethoxysilane, or with a more promising use of thioanhydrides for ease in stibnite deposition. With these changes, futures studies using ultraviolet photoelectron-spectroscopy and UV-Vis surface spectroscopy could be used to measure conductance to ensure films maintain the bandgap energy that stibnite should have for its semiconductive applications.

References

[1] Azizian, Saeid, and Maryam Hemmati. “Surface Tension of Binary Mixtures of Ethanol + Ethylene Glycol from 20 to 50 °C.” *Journal of Chemical & Engineering Data*, vol. 48, no. 3, 2003, pp. 662–663., https://doi.org/10.1021/je025639s.

[2] *Best Research-Cell Efficiencies*. NREL Transforming Energy. Accessed 27 Apr. 2022.

[3] Carl, Alexander D., et al. “Synthesis and Characterization of Alkylamine-Functionalized Si(111) for Perovskite Adhesion with Minimal Interfacial Oxidation or Electronic Defects.” *ACS Applied Materials & Interfaces*, vol. 9, no. 39, 2017, pp. 34377–34388., https://doi.org/10.1021/acsami.7b07117.

[4] Dimatix Fujifilm. *Materials Printer & Cartridge DMP-2800 Series Printer & DMC-11600 Series Cartridge*, Dimatix Fujifilm, Santa Clara, CA.

[5] Doriron, Curtis W. *MODIFICATION OF BACK-SURFACE CONTACTS TO ANTIMONY SULFIDE ACTIVE LAYERS USING CARRIER-SELECTIVE THIONATED PERYLENE DERIVATIVES FOR IMPROVED PHOTOVOLTAIC PERFORMANCE*, May 2019, pp. 1–41.

[6] Duan, Shuming, et al. “Scalable Fabrication of Highly Crystalline Organic Semiconductor Thin Film by Channel-Restricted Screen Printing toward the Low-Cost Fabrication of High-Performance Transistor Arrays.” *Advanced Materials*, vol. 31, no. 16, 2019, p. 1807975., https://doi.org/10.1002/adma.201807975.

[7] *Ethylene Glycol EGL - NOAA*. https://cameochemicals.noaa.gov/chris/EGL.pdf.

[8] Fujisawa, Jun-ichi, et al. “Comparative Study of Conduction-Band and Valence-Band Edges of tio2, SrTiO3, and BATIO3 by Ionization Potential Measurements.” *Chemical Physics Letters*, vol. 685, 2017, pp. 23–26., https://doi.org/10.1016/j.cplett.2017.07.031.

[9] “Viscosity, Surface Tension, Specific Density and Molecular Weight of Selected Liquids.” *Viscosity, Surface Tension, Specific Density and Molecular Weight of Selected Liquids (Sort by Surface Tension)*, DIVERSIFIED Enterprises, https://www.accudynetest.com/visc_table.html?sortby=sort_surface_tension.

[10] Katz, Howard E. “Recent Advances in Semiconductor Performance and Printing Processes for Organic Transistor-Based Electronics.” *Chemistry of Materials*, vol. 16, no. 23, 2004, pp. 4748–4756., https://doi.org/10.1021/cm049781j.

[11] Kim, S.-Y., et al. “High-Resolution Electrohydrodynamic Inkjet Printing of Stretchable Metal Oxide Semiconductor Transistors with High Performance.” *Nanoscale*, vol. 8, no. 39, 12 Sept. 2016, pp. 17113–17121., https://doi.org/10.1039/c6nr05577j.

[12] Kondrotas, Rokas, et al. *Sb2S3 Solar Cells*, vol. 2, 16 May 2018, pp. 857–878.

[13] McCabe, Nick. "Viscosity and Stoke's Equation." *UCSC Physics Demonstration Room*, University of California Santa Cruz, https://ucscphysicsdemo.sites.ucsc.edu/physics-5b6b-demos/viscosity-and-stokes-equation/.

[14] Messina, Sarah, et al. "Antimony Sulfide Thin Films in Chemically Deposited Thin Film Photovoltaic Cells." *Thin Solid Films*, vol. 515, no. 15, 2007, pp. 5777–5782., https://doi.org/10.1016/j.tsf.2006.12.155.

[15] *Physical Properties - Airgas Specialty Products*. https://airgasspecialtyproducts.com/wp-content/uploads/2016/02/Physical_Properties-1.pdf.

[16] Prinz, A.V., et al. "Semiconductor Micro- and Nanoneedles for Microinjections and Ink-Jet Printing." *Microelectronic Engineering*, Elsevier, 15 Mar. 2003, https://www.sciencedirect.com/science/article/pii/S0167931703001394.

[17] Savadogo, O., and K. C. Mandal. "Characterizations of Antimony Tri-Sulfide Chemically Deposited with Silicotungstic Acid." *Journal of The Electrochemical Society*, vol. 139, no. 1, 1992, https://doi.org/10.1149/1.2069211.

[18] Sedov, I.A., et al. "Enthalpies and Gibbs Free Energies of Solvation in Ethylene Glycol at 298 K: Influence of the Solvophobic Effect." *Fluid Phase Equilibria*, Elsevier, 25 June 2013, https://www.sciencedirect.com/science/article/pii/S0378381213003038.

[19] Shockley, William, and Hans Queisser. "Detailed Balance Limit of Efficiency of P–N Junction Solar Cells." *Renewable Energy*, 2018, pp. 35–54., https://doi.org/10.4324/9781315793245-44.

[20] Sreedevi, Gedi, and Kotte Tulasi Ramakrishna Reddy. "Properties of Tin Monosulphide Films Grown by Chemical Bath Deposition." *Conference Papers in Energy*, vol. 2013, 2013, pp. 1–5., https://doi.org/10.1155/2013/528724.

[21] "Triethanolamine." *National Center for Biotechnology Information. PubChem Compound Database*, U.S. National Library of Medicine, https://pubchem.ncbi.nlm.nih.gov/compound/triethanolamine#section=Decomposition.

[22] Wang, Qinqin, et al. "Study on the Cleaning Process of n+-Poly-Si Wraparound Removal of Topcon Solar Cells." *Solar Energy*, vol. 211, 2020, pp. 324–335., https://doi.org/10.1016/j.solener.2020.09.028.

[23] Wanic, Michał, et al. "Surface Tension of Ethylene Glycol-Based Nanofluids Containing Various Types of Nitrides." *Journal of Thermal Analysis and Calorimetry*, vol. 139, no. 2, 2019, pp. 799–806., https://doi.org/10.1007/s10973-019-08512-1.

Appendix A: Structure of Stibnite

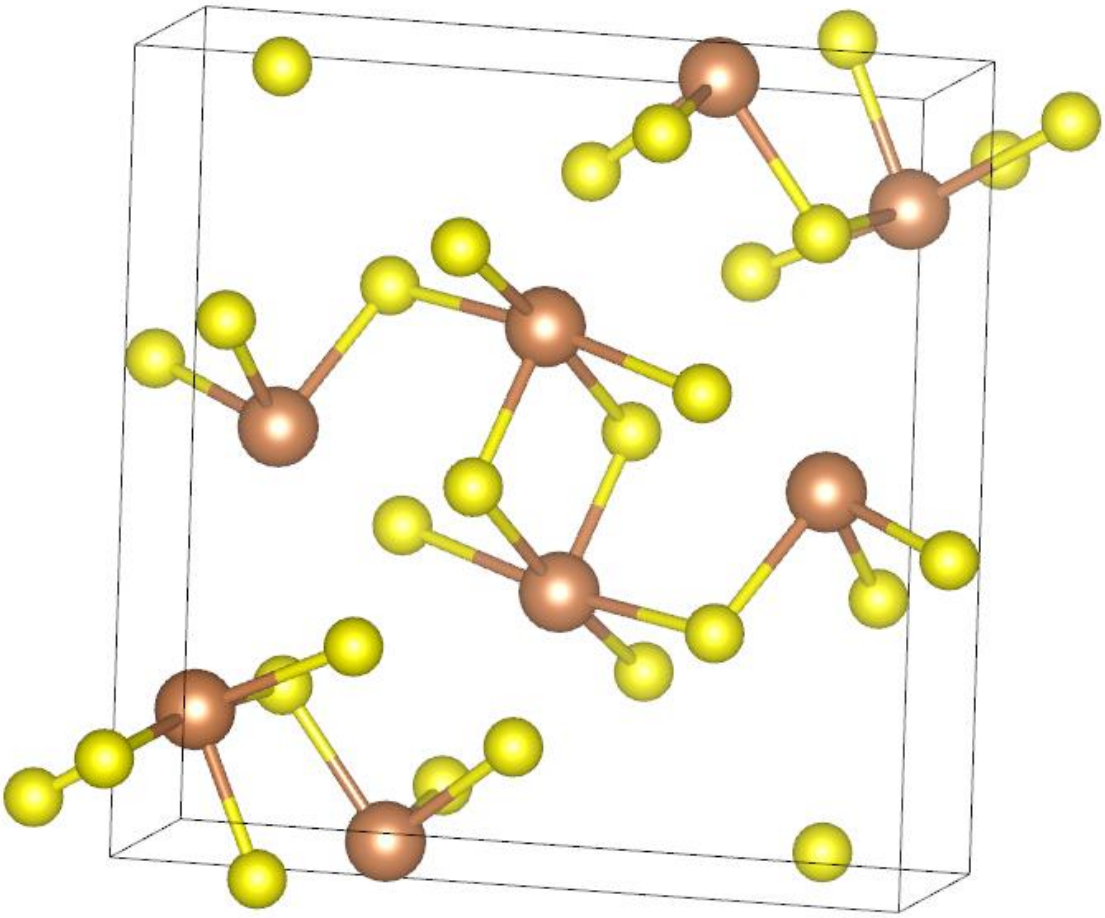

Figure 13: Unit Cell of Stibnite. Orange balls represent antimony and yellow balls represent sulfur

Appendix B: Predicted Powder X-Ray Diffraction Trace for Stibnite

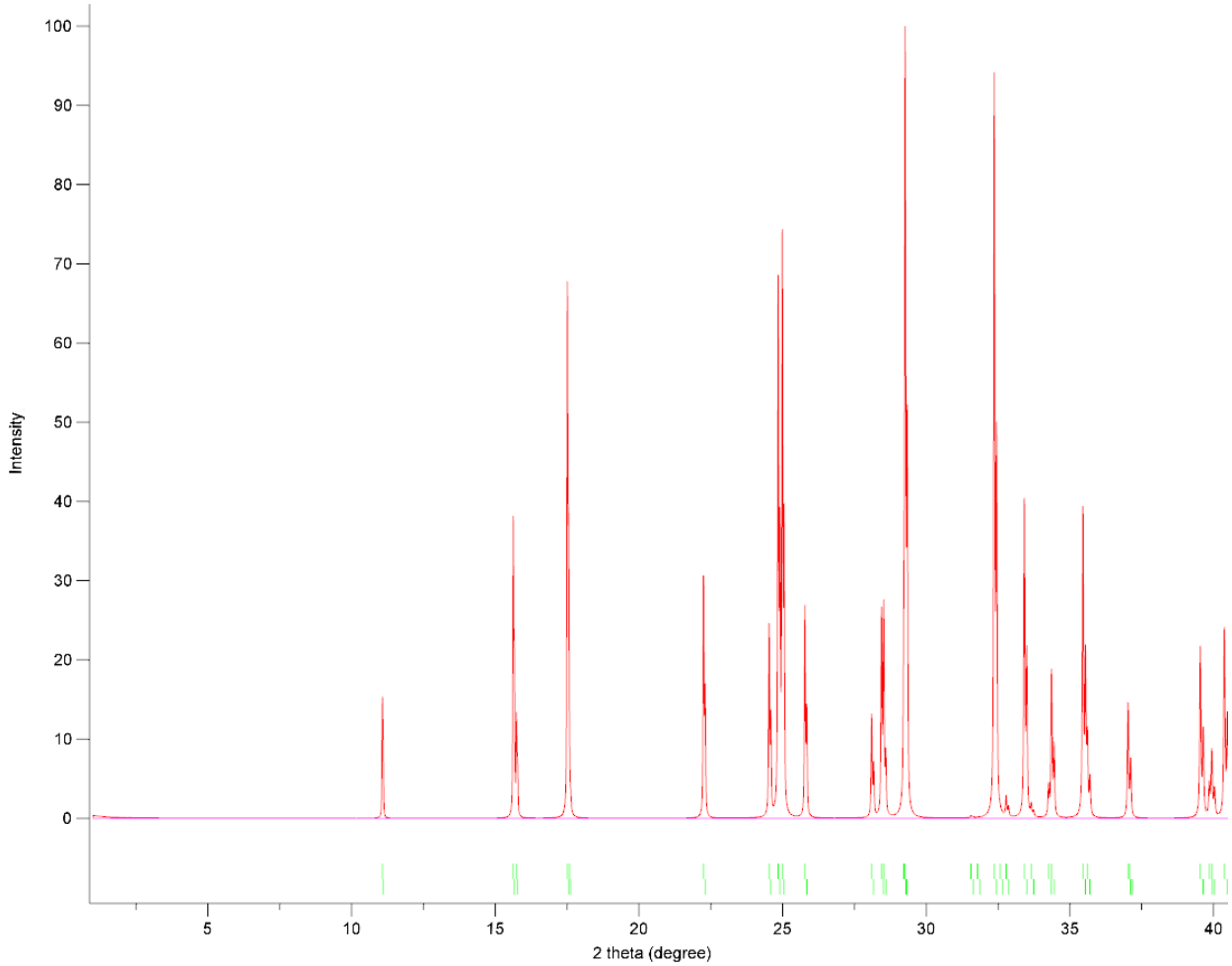

Figure 14: Predicted powder x-ray diffraction trace of stibnite calculated by the computer program VESTA.